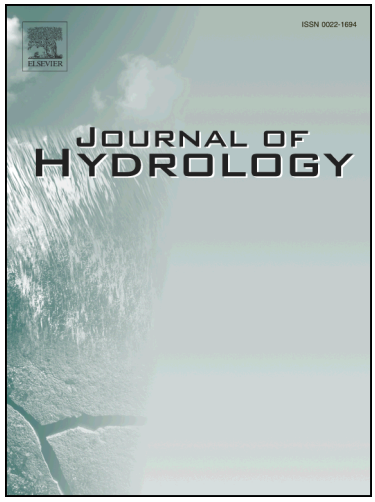
**This is the accepted manuscript version of the contribution published as:**

**Binder, M.**, Burghardt, D., **Engelmann, C.**, **Tritschler, F.**, Simon, E., Prommer, H., **Dietrich, P.**, Liedl, R., **Händel, F.** (2019):
Suitability of precipitation waters as semi-artificial groundwater tracers
*J. Hydrol.* **577** , art. 123982

**The publisher's version is available at:**

http://dx.doi.org/10.1016/j.jhydrol.2019.123982

Journal Pre-Proof




Research papers

# Suitability of precipitation waters as semi-artificial groundwater tracers

Martin Binder, Diana Burghardt, Christian Engelmann, Felix Tritschler, Elisabeth Simon, Henning Prommer, Peter Dietrich, Rudolf Liedl, Falk Händel

PII: S0022-1694(19)30702-4
DOI: https://doi.org/10.1016/j.jhydrol.2019.123982
Reference: HYDROL 123982

To appear in: *Journal of Hydrology*

Received Date: 1 April 2019
Revised Date: 22 July 2019
Accepted Date: 23 July 2019

Please cite this article as: Binder, M., Burghardt, D., Engelmann, C., Tritschler, F., Simon, E., Prommer, H., Dietrich, P., Liedl, R., Händel, F., Suitability of precipitation waters as semi-artificial groundwater tracers, *Journal of Hydrology* (2019), doi: https://doi.org/10.1016/j.jhydrol.2019.123982

This is a PDF file of an article that has undergone enhancements after acceptance, such as the addition of a cover page and metadata, and formatting for readability, but it is not yet the definitive version of record. This version will undergo additional copyediting, typesetting and review before it is published in its final form, but we are providing this version to give early visibility of the article. Please note that, during the production process, errors may be discovered which could affect the content, and all legal disclaimers that apply to the journal pertain.

© 2019 Published by Elsevier B.V.

JOURNAL PRE-PROOF

# Suitability of precipitation waters as semi-artificial groundwater tracers

Martin Binder [a,b,*], Diana Burghardt [a], Christian Engelmann [a,b], Felix Tritschler [a,c], Elisabeth Simon [a], Henning Prommer [d,e], Peter Dietrich [c,f], Rudolf Liedl [a], Falk Händel [a,c]

[a] Technische Universität Dresden, Institute of Groundwater Management, Bergstraße 66, D-01069 Dresden, Germany

[b] Helmholtz-Centre for Environmental Research - UFZ, Department Environmental Informatics, Permoserstraße 15, D-04318 Leipzig, Germany

[c] Helmholtz-Centre for Environmental Research - UFZ, Department Monitoring and Exploration Technologies, Permoserstraße 15, D-04318 Leipzig, Germany

[d] CSIRO Land and Water, Private Bag 5, Wembley, WA 6913, Australia

[e] University of Western Australia, School of Earth Sciences, Crawley, WA 6009, Australia

[f] University of Tübingen, Department of Geosciences, Hölderlinstr. 12, D-72074 Tübingen, Germany

* Corresponding author (martin.binder@tu-dresden.de and martin.binder@ufz.de, Tel: +49-351-463-42557, Fax: +49-351-463-42552, ORCID: 0000-0003-2296-0582)

## Abstract

In this study the suitability of precipitation waters as semi-artificial and multi-component groundwater tracers is investigated and potential applications as well as limitations are discussed. Specifically, we analyzed their migration behavior during laboratory-scale experiments with groundwater-saturated porous media. Artificially $^{2}H$- and $^{18}O$-labelled water as well as natural precipitation waters were injected into sediment-packed columns and traced via stable isotope analysis. Their migration behavior was compared to that of widely used tracers. These flow-through experiments were underpinned by a batch reactor study and by hydrogeochemical modeling. While most artificial isotope applications showed a high stability and conservative transport behavior for all tested sediments, the breakthrough curves observed in some experiments with rain and snowmelt were unsteady. This was most likely caused by the small ratio between the tracer's isotopic difference compared to the background signal and the available analytical precision. The minimum ratio required for effectively reducing uncertainties during data evaluation showed to depend significantly on experimental conditions but should not decrease below ~10 during peak breakthrough and preferably be higher. Furthermore, our study illustrates that measurements based on using the precipitation waters' inherent low electrical conductivity

can be significantly biased by water-sediment reactions. The batch study and reactive transport simulations confirmed this observation while revealing mineral reactions and, to a minor extent, also ion exchange as the underlying processes.

**Keywords**

precipitation water; tracer; groundwater; deuterium; oxygen-18; electrical conductivity

## 1. Introduction

In hydrogeology, tracer tests are routinely used to reveal the fundamental transport characteristics of aquifers (Davis et al., 1980). The value of any tracer, whether intentionally applied to the subsurface (‘artificial’ tracer) or naturally abundant (‘environmental’ tracer), depends on many different factors, including the tracer characteristics, the aquifer characteristics, and the employed experimental design. Most tracer test techniques rely on the assumption of a strictly conservative behavior of the traced signal (Davis et al., 1980; Käss, 2004), i.e., the tracer should be physically and chemically inert such that it mimics the migration of the water molecules (Becker and Coplen, 2001). Additionally, tracers should be non-toxic, easy-to-use, and clearly distinguishable from the ambient groundwater (e.g., Käss, 2004), i.e., a sufficiently pronounced signal-to-noise ratio (SNR) is required.

Among others, a wide selection of salts such as sodium chloride (NaCl) or potassium bromide (KBr), dyes (e.g., sodium fluorescein, i.e., uranine), as well as stable or radioactive isotopes, but alternatively also sum parameters such as electrical conductivity (EC) can be employed in artificial tracer studies (Davis et al., 1980; Käss, 2004). Further traceable substances such as persistent pharmaceutical compounds (Arye et al., 2011) or properties such as temperature (Greskowiak et al., 2006; Seibert et al., 2014) have been successfully used as environmental tracers, e.g., in the context of monitoring Soil Aquifer Treatment or Managed Aquifer Recharge systems. However, under unfavorable conditions, most of these tracers can change their expected behavior due to environmental factors and their variability.

For example, the inert behavior of uranine persists only for a limited groundwater pH range (Käss, 2004).

The stable isotopes of the water molecule elements are deemed to be the most ideal water tracers as they "resemble the water [molecule] both physically and chemically" (Becker and Coplen, 2001). Signatures of natural waters, which are typically reported as Delta notations, i.e., as $\delta^{2}H$ (deuterium) and as $\delta^{18}O$ (oxygen-18) in '‰ vs. VSMOW2' (Vienna Standard Mean Ocean Water), depend strongly on climatic factors (e.g., Mook and de Vries, 2001). Therefore, they can vary significantly with covered ranges of $\Delta(\delta^{2}H) \approx 400‰$ and $\Delta(\delta^{18}O) \approx 40‰$ (Dansgaard, 1964), respectively. Numerous environmental tracer studies have exploited such differences in the isotopic fingerprint for, among others, recharge estimation (e.g., Adomako et al., 2010), flow and discharge pattern identification (e.g., James et al., 2000) as well as the analysis of groundwater origins and evolution (e.g., Tsujimura et al., 2007). Studies that employed artificial isotope labelling relied mostly on deuterium oxide ($^{2}H_2O$), i.e., artificially $^{2}H$-enriched water to determine flow and transport parameters in aquifers (e.g., Garnier et al.,1985; Maloszewski et al., 1999; Luhmann et al., 2012) and to actively investigate infiltration processes in the vadose zone (e.g., Hangen et al., 2005; Mali et al, 2007; Schoen et al., 1999). Koeniger et al. (2010) also used artificially $^{18}O$-enriched water, i.e., $H_2{}^{18}O$ to investigate snowmelt infiltration.

Recently, precipitation waters were employed as injection waters in two artificial tracer tests on small field scale (Binder et al., 2019a; Tritschler et al., 2019), thereby intentionally exploiting the existing inherent offset of $\delta^{2}H$, $\delta^{18}O$, and EC as detectable entities. In Binder et al. (2019a), for example, the isotopes' conservative behavior of a significantly depleted snowmelt was compared to variations in the EC that were simultaneously induced by the active injection of meltwater into a fluviatile aquifer. Both isotope signal components were recovered during extraction in the form of clearly measurable perturbations with SNRs during the peak between ~21 ($\delta^{2}H$) and ~24 ($\delta^{18}O$). These results, however, indicate that the currently available precision of stable isotope analysis may limit the information content of a breakthrough signal in cases where the isotopic shift is less pronounced. Furthermore, the

observed behavior of the EC signal, in particular a reduced peak value, suggested that geochemical reactions may have influenced the migration. Both aspects need to be better understood in order to clarify the usefulness of precipitation waters as 'active' multi-component tracers for aquifers, i.e., fully water-saturated porous media. Therefore, we performed comparative laboratory-scale experiments with controlled precipitation water applications to investigate their stability and to what extent they behaved truly conservatively. Finally, we performed transport simulations to investigate measurement uncertainties and to explain observed EC modifications.

## 2. Study site

The site selected for this study is located in Pirna, Saxony, Germany, in close vicinity to the Elbe River (Figure 1). Pirna is characterized by a humid-temperate climate with an annual precipitation slightly below 700 mm (e.g., Tritschler et al., 2019).

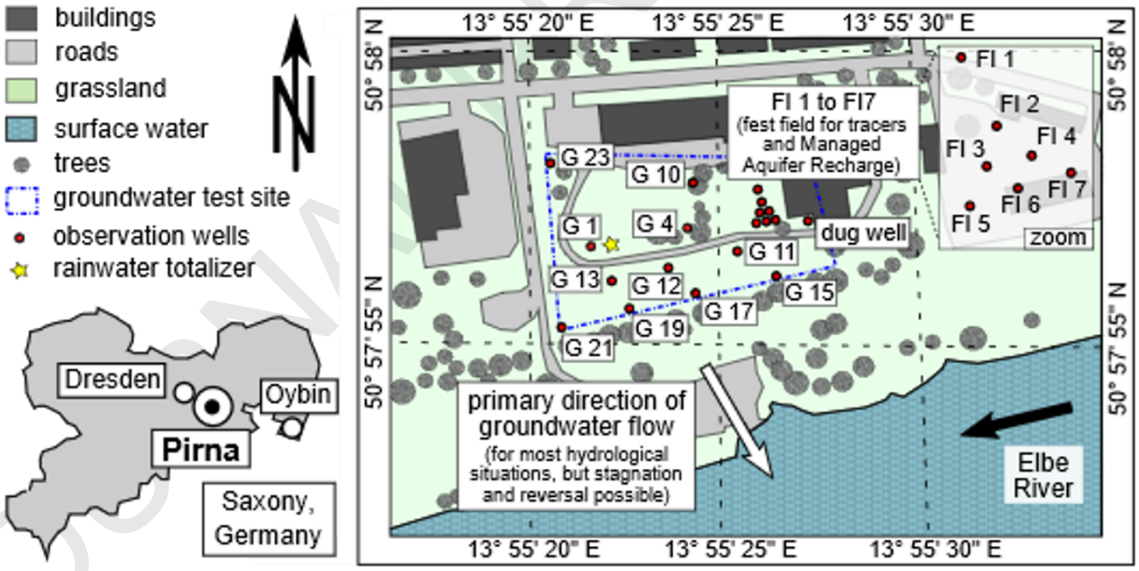



**Figure 1.** Scheme of the investigated study site in Pirna, Saxony, Germany, as well as approximate positions of precipitation water sampling points in Saxony (Pirna, Dresden and Oybin).

Four types of sediments (Table 1) were prepared to represent the characteristics of this site's lithology, with a particular focus on the sediments from the upper semi-confined aquifer. This aquifer zone consists of two distinct sub-sections (Dietze and Dietrich, 2012; Händel et al., 2016): (i) an overlying section of relatively low permeability (hydraulic conductivities, i.e., $K$ values are below ~$10^{-6}$ m/s) with anthropogenic fillings and varying

content of fines originating from flood events as well as (ii) an underlying highly permeable section (*K* values mostly between ~$10^{-4}$ m/s and ~$10^{-3}$ m/s) consisting of sands and gravel.

**Table 1:** Sediment composition and characteristics. Labels after Unified Soil Classification System.

| sediment label and abbreviation | well-graded sand (SW) | poorly-graded sand (SP) | silty sand (SM) | silty sand with clay (SM-SC) |
|---|---|---|---|---|
| components [a] (approximate mass shares given in eights) | 8/8×PR | 6/8×PR, 2/8×HE | 4/8×PR, 4/8×HE | 6/8×PR, 1/8×HE, 1/8×LP |
| sand and gravel content (mass-%) | 100 | 93–94 | 88–89 | 86–87 |
| silt and clay content (mass-%) | 0 | 6–7 | 11–12 | 13–14 (~2% kaolinite clay) |
| coefficient of uniformity $C_U = d_{60\%}/d_{10\%}$ | 3 | 5 | 13 | 19 |
| saturated hydraulic conductivity at 10 °C (m/s) [b] | 3–4×$10^{-4}$ | 1–2×$10^{-6}$ | 8×$10^{-7}$ | 3×$10^{-7}$ |
| total porosity (vol.-%) [c] | 34.7 | 29.1 | 30.4 | 32.1 |

[a] abbreviations for the material' origins are: PR for Pratzschwitz, HE for Heidenau and LP is the loam powder

[b] based on permeameter tests (falling head method), [c] based on bulk and grain density measurements (for the columns)

All materials were obtained from nearby gravel/sand pits (Pratzschwitz, Germany) and excavations (Heidenau, Germany). Where needed, samples were amended with kaolinite loam powder to more closely mimic the fines found at the study site, especially with respect to the particle size distribution. Note that multiple detrimental impacts on the stability of uranine such as a slight sorption-desorption hysteresis were previously observed for these sediments, especially for the Heidenau material component (Fichtner et al., 2015). A fifth sediment type (not shown in Table 1), comparable to the kaolinite sample, was included to identify the potential influence of clay-type (e.g., Brady and Weil, 2002) on tracer stability. This sediment contained ~2% montmorillonite clay instead of kaolinite, using an artificial material called 'Friedländer Blauton', which was pretreated with sodium bicarbonate, i.e., $NaHCO_3$ during the manufacturing process.

Four precipitation water samples (Table 2) were selected to act as proxies for the multitude of waters in the region of Central and Eastern Saxony (Figure 1: small grey map).

The employed totalizers were protected from evaporation losses and other environmental influences by using a combination of the table tennis ball and paraffin oil methods, as suggested by the International Atomic Energy Agency (IAEA/GNIP, 2014). Both rain samples were characterized by comparably low ionic strengths (0.4 to 0.6 mmol/$kg_W$) and low buffering capacities (e.g., Burton and Pitt, 2001). Contrary, the two snow samples had elevated ionic strengths (2.3 to 3.2 mmol/$kg_W$). Those can be attributed to previous winter service activities in the sampled area.

**Table 2:** Natural precipitation samples from Central and Eastern Saxony, Germany.

| precipitation water type/origin | sampling point coordinates | sampling altitudes (m.a.s.l) | sampling period | sampling method |
|---|---|---|---|---|
| summer rain (Pirna, study site) | 50°57'57" N, 13°55'24" E | 118 | 05-06/2016 | rainwater totalizer (star in Figure 1) |
| old snow (Dresden) | 51°01'41" N, 13°43'48" E | 142 | 01/2016, ~4 days after a snowfall event | direct collection; melted while avoiding contact to atmosphere |
| new snow (Dresden) | 51°01'41" N, 13°43'48" E | 142 | 01/2017, almost immediately after a snowfall event | same as for old snow |
| mountain rain (Oybin) | 50°49'24" N, 14°46'0" E | 424 | 06-09/2013 | rainwater totalizer |

Using a 2" submersible pump (Co. Grundfos), groundwater was extracted from observation well FI 7 (Figure 1: tracer test field), hereafter referred to as 'Pirna groundwater'. It was employed as reference water. The groundwater sample has an ionic strength of 8.7 mmol/$kg_W$; its chemical composition is given in ESM S1. Note that further samples from G1 to G23 were included in the analysis. Both snowmelt samples are isotopically depleted relative to the groundwater, while the rain samples are isotopically enriched.

Additionally, artificial isotope labelling was applied. For that purpose, small amounts of $^2H_2O$ (Co. Deutero, ~4 µL/L, isotopic purity of 99.9at-%) and $H_2{}^{18}O$ (Co. Sigma-Aldrich, ~120 µL/L, 10.0at-%,) were equilibrated with groundwater to simulate isotope values of

precipitation as observed on-site. Here, deviations relative to the groundwater range from -30‰ to +40‰ for $\delta^2H$ and from -4‰ to +6‰ for $\delta^{18}O$ (Tritschler et al., 2019). From this data pool, a sample from a heavy rainfall event in late summer 2016 was selected to serve as template. Aside from the artificial isotope labeling, this 'synthetic rain' and the groundwater are identical which allowed this study to focus on signature changes.

## 3. Laboratory experiments

### *3.1. Overview of the experimental setup*

The laboratory investigations consisted of two main parts. First, a batch reactor study was performed to assess the hydrochemical and isotopic short-term stability of natural and synthetic precipitation waters in contact with the test sediments. Then, tracer experiments in sediment-packed columns were performed to assess their transport behavior. Uranine, NaCl and KBr were employed as reference tracers.

All experiments were placed in a climate chamber (Co. Viessmann) to simulate groundwater temperatures and to create a dark environment avoiding UV degradation of uranine. All water samples were stored in gas-dense composite material pouches made of aluminum, polyethylene and polypropylene layers (Co. Tesseraux Spezialverpackungen). In order to reduce any bias induced by potential changes in isotope signatures and chemical compositions during storage, all reported values in this study refer to conditions found shortly, i.e., within a few hours before the start of the respective experiments. Experimental setup schemes are provided in the Electronic Supplementary Material (ESM) S1.

$\delta^2H$ and $\delta^{18}O$ values were determined using a high-precision isotope ratio mass spectroscopy (IRMS) system (MAT 253, Co. Thermo Fisher Scientific) coupled to a high-temperature pyrolysis furnace (Co. HEKAtech). Water salinities were measured using a 4-pole EC sensor (Co. WTW), while a bromide ion-selective electrode (ISE, Co. WTW) and an ion-chromatography system (IC, Co. Dionex) were employed for ion analysis. Uranine-induced fluorescence was determined using a spectral fluorimeter (Co. Albilia).

### *3.2. Short-term batch stability experiments*

3.2.1 Experimental procedure

For the 24-hour short-term stability tests, the sediments were air-dried (pore water contents below ~2%) and filled into borosilicate glass bottles. Then, either labelled or non-labelled waters (the latter as reference) were added in a ratio of 0.5 $kg_{sediment}/L_{water}$ as suggested for natural sediments (e.g., Limousin et al., 2007). Applied concentration levels, isotope signatures and precipitation water mixtures are listed in Table 3. After set-up, all sediment-water suspensions were equilibrated using an overhead shaker (~24 h, ~6 rpm). Extraction of pore water was performed by centrifugation (~5000 rpm) followed by filtration through a CME membrane (cellulose mixed ester, 0.2 µm). The extracts were analyzed for their hydrochemical compositions and isotope signatures.

**Table 3.** Initial isotope and selected physicochemical parameters of the short-term batch experiments. All isotope Delta values are referenced to VSMOW2. The given ranges comprise multiple sub-samples (NaCl: 3x; KBr: 4x; uranine: 4x; natural precipitation (as listed in Table 2): one unaltered sub-sample plus one 1:1 a-priori mixture with groundwater each).

| injected substance | measured values (unit) | applied 'concentrations' |
|---|---|---|
| *background water* | | |
| Pirna groundwater | EC (µS/cm) | 542 |
| | KBr concentration (mg/L) | <1 |
| | uranine concentration (µg/L) | <1 |
| | $\delta^2H$ (‰) | -61.1 |
| | $\delta^{18}O$ (‰) | -8.2 |
| *reference tracers and precipitation waters* | | |
| NaCl | EC (µS/cm) | 3040 to 14220 |
| KBr | KBr concentration (mg/L) | 120.3 to 463.3 |
| Uranine | uranine concentration (µg/L) | ~160 to ~670 |
| low-mineralized water | EC (µS/cm) | 14 |
| synthetic rain | $\delta^2H$ (‰) | -37.4[a] and -49.5[b] |
| | $\delta^{18}O$ (‰) | -3.2[a] and -5.6[b] |
| natural precipitation: summer/mountain rain | EC (µS/cm) | 26[a] to 304[b] |
| | $\delta^2H$ (‰) | -50.7[a] to -58.9[b] |
| | $\delta^{18}O$ (‰) | -6.6[a] to -7.8[b] |
| natural precipitation: old/new snow | EC (µS/cm) | 140[a] to 386[b] |
| | $\delta^2H$ (‰) | -101.3[a] to -67.0[b] |

| | | |
|---|---|---|
| | $\delta^{18}O$ (‰) | -14.1[a] to -10.4[b] |

[a] direct application, [b] application in an a-priori mixture with Pirna groundwater (~1:1 mixture fractions)

3.2.2 Data analysis

The short-term stabilities were determined by first calculating the residuals between the initial concentration ($C_{init}$) and the concentration recorded after 24 h ($C_{equil}$). A dimensionless batch stability criterion, hereafter referred to as $Y_{Batch}(B)$, was then defined using an adapted version of the normalized root-mean-square error with

$$Y_{\mathrm{Batch}}(B) = \sqrt{\frac{\sum_{i=1}^{u}\left(\frac{C_{\mathrm{equil},i}}{C_{\mathrm{init},i}} - 1\right)^2}{u}} \quad (1)$$

for a total of $u$ samples related to a specific detection parameter $B$ (e.g., $\delta^2H$). A low value for $Y_{Batch}(B)$ indicates a high stability for the analyzed substance (with '0' equaling quasi-perfect stability). EC values were considered in a logarithmic form as these cover three orders of magnitude in the experiments. As most laboratories report stable isotope analysis results in Delta notation, isotope values were also considered in this notation and not as real abundancies of the rare isotope.

*3.3. Column transport experiments*

3.3.1 Experimental procedure

A series of column experiments was conducted to assess the suitability of precipitation waters as active tracers under consideration of the various technical limitations such as IRMS precision. Four separate columns (ID 7 cm, length 40 cm) were wet-packed with the test sediments. After set-up and prior to the first tracer application, all columns were slowly flushed with non-labelled Pirna groundwater for ~30 total pore volumes to ensure that complete water saturation as well as geochemical equilibrium conditions were attained. Furthermore, custom-build automatic sampling devices were attached directly to the column effluent ends to minimize sampling errors.

First, the transport performance of the synthetic rain, i.e., the artificial mixture of $^2H_2O$ and $H_2{}^{18}O$ was compared for all four sediments against the reference tracer substances

(Table 4). For this, three experiments (E1 – E3) injecting short pulses of NaCl (E1), synthetic rain (E2) and lastly KBr and uranine (E3) were performed. For the subsequent experiments, one natural snowmelt sample (E4) and two natural rain samples (E5 and E6) were successively injected into the column packed with the well-graded sand (Table 4).

**Table 4.** Tracer types and measured parameters in the column transport experiments E1 to E6. Initial values refer to the conditions after continuous injection of Pirna groundwater. All isotope Delta values are referenced to VSMOW2.

| test series | tracer / application mode | measured parameter (unit) | tracer value (column inflow) | background value (column outflow, mean initial values) | | | |
|---|---|---|---|---|---|---|---|
| | | | | SW | SP | SM | SM-SC |
| E1 (EC-based tracer) | NaCl | EC (µS/cm) | 6760±50 (~3.3 g/L) | 550 | 546 | 552 | 600 |
| E2 (synthetic rain) | $^{2}H_2O$ | $\delta^{2}H$ (‰) | -35.6 | -62.3 | -61.9 | -61.3 | -61.2 |
| | $H_2{}^{18}O$ | $\delta^{18}O$ (‰) | -2.9 | -8.8 | -8.7 | -8.5 | -8.5 |
| E3 (dye- and ion-based tracer) | KBr | KBr concentration (mg/l) | 100 | 0.5 | 0.9 | 0.9 | 1.3 |
| | uranine | uranine concentration (µg/L) | ~580 | <1 | <1 | <1 | <1 |
| E4 (old snow) | melted, direct application | EC (µS/cm) | 139 | 542 | - | - | - |
| | | $\delta^{2}H$ (‰) | -74.0 | -61.4 | - | - | - |
| | | $\delta^{18}O$ (‰) | -11.1 | -8.7 | - | - | - |
| E5 (mountain rain) | direct application | EC (µS/cm) | 37 | 534 | - | - | - |
| | | $\delta^{2}H$ (‰) | -47.6 | -61.4 | - | - | - |
| | | $\delta^{18}O$ (‰) | -5.4 | -8.4 | - | - | - |
| E6 (summer rain) | direct application | EC (µS/cm) | 25 | 544 | - | - | - |
| | | $\delta^{2}H$ (‰) | -50.8 | -60.9 | - | - | - |
| | | $\delta^{18}O$ (‰) | -7.3 | -8.7 | - | - | - |

SW … well-graded sand, SP … poorly-graded sand, SM … silty sand, SM-SC … silty sand with kaolinite clay

The intermediate step that employed the synthetic rain sample (E2) was included to focus on elucidating the migration behavior of the isotopes, while avoiding, for example, the impact of mineral reactions due to chemical differences between tracer and background. The new snow sample was not injected, as the focus was not on extreme scenarios but on

assessing precision-related uncertainties. However, a column flow experiment employing an also noticeably depleted snowmelt sample, with initial tracer SNRs of ~61 ($\delta^2H$) and ~55 ($\delta^{18}O$), is documented in Binder et el. (2019a).

All experiments consisted of 24-h tracer/precipitation injections, followed by a continuous injection of unlabeled groundwater until the initial equilibrium conditions were restored. Mean Darcy velocities (Table 5) varied between the columns due to the significant differences in hydraulic conductivity and varying contact pressures of the separate flow channels of the peristaltic pump used (Co. Ismatec). The Darcy velocities that resulted from this setup reflect the lower range of the velocities that typically prevail at our site.

**Table 5.** Darcy velocities and sampling procedures for the column displacement experiments.

| | **experiments E1 to E3** | **experiments E4 to E6** |
|---|---|---|
| | *approximate Darcy velocities (cm/d)* | |
| **well-graded sand** | 6.8 | 7.6 |
| **poorly-graded sand** | 6.5 | - |
| **silty sand** | 6.7 | - |
| **silty sand with kaolinite clay** | 5.4 | - |
| | *sampling procedure* | |
| **time interval** | ~8 h | ~4 h |
| **focus** | complete runtime (8 days) | focus on breakthrough only |

3.3.2 Data analysis

Sampling times as well as the averaged analytical values (‘*a*’ in Eqs. 2 and 3) were considered on normalized scales to allow for a direct comparison. As the initial SNRs were sufficiently pronounced in the experiments E1 to E3, measurement errors were neglected for observed concentrations, for sum parameters (here: EC), and for stable isotope values, i.e.,

$$\tilde{C}_{\mathrm{mean}} \approx \frac{a_{\mathrm{sample}} - a_{\mathrm{background}}}{a_{\mathrm{tracer}} - a_{\mathrm{background}}} \quad . \tag{2}$$

For the stable isotope values observed in the experiments E4 to E6, which are characterized by much lower SNRs, the analytical precision of the employed IRMS system (*'b'* in Eq. 3 with ±1.0‰ for $\delta^2H$ and ±0.2‰ for $\delta^{18}O$) was included to span a bandwidth, i.e.,

$$[\tilde{C}_{\min}, \tilde{C}_{\max}] = \frac{(a_{\text{sample}} \pm b_{\text{sample}}) - (a_{\text{background}} \pm b_{\text{background}})}{(a_{\text{tracer}} \pm b_{\text{tracer}}) - (a_{\text{background}} \pm b_{\text{background}})} \quad . \tag{3}$$

After normalization, all observations were evaluated for plausibility by reproducing the experimentally obtained breakthrough curves (BTC) with a 1-D analytical model. Specifically, the dual domain mass transfer approach (DDMT; van Genuchten and Wierenga, 1976) was employed for solute transport simulation. Four relevant transport parameters were determined while minimizing the residuals between simulated and measured BTCs: mobile porosity, immobile porosity, longitudinal dispersivity and the dual-domain mass transfer coefficient. In order to effectively quantify uncertainties introduced by the different tracer signals, a comparative statistical analysis was done by calculating four selected quality criterions, specifically the root-mean-square-error (RMSE), the mean-absolute-error (MAE), the weighted coefficient of determination ($wR^2$) and the index of agreement, as well as by performing a linear regression analysis for all possible tracer combinations. Further details are provided in ESM S2 (parameter estimation) and ESM S3 (statistical analysis).

## 4. Experimental results and basic analysis

### *4.1. Short-term batch stability experiments*

The observed $\delta^2H$ values before and after equilibration with all tested sediments were very similar (Figure 2a), suggesting that neither the artificially isotope-labelled waters nor the natural precipitation water were affected by any detrimental impacts within the selected experimental duration of 24 h ($Y_{\text{Batch}}(\delta^2H) < 0.01$). This finding is expected to remain valid for applications with slightly increased experimental periods, as no fractionation processes should be relevant for this short timescale aside from mixing processes with remains of indigenous pore water. Similar findings apply to the measured $\delta^{18}O$ values (Figure 2b),

although slight deviations from the 1:1 line were observed, especially in the range between -8‰ and -11.5‰. This leads to a slightly higher value for $Y_{Batch}(\delta^{18}O)$ of ~0.02. However, as most samples remained within the error margin of the IRMS precision, $\delta^{18}O$ can also be considered as a highly stable tracer for short-term applications.

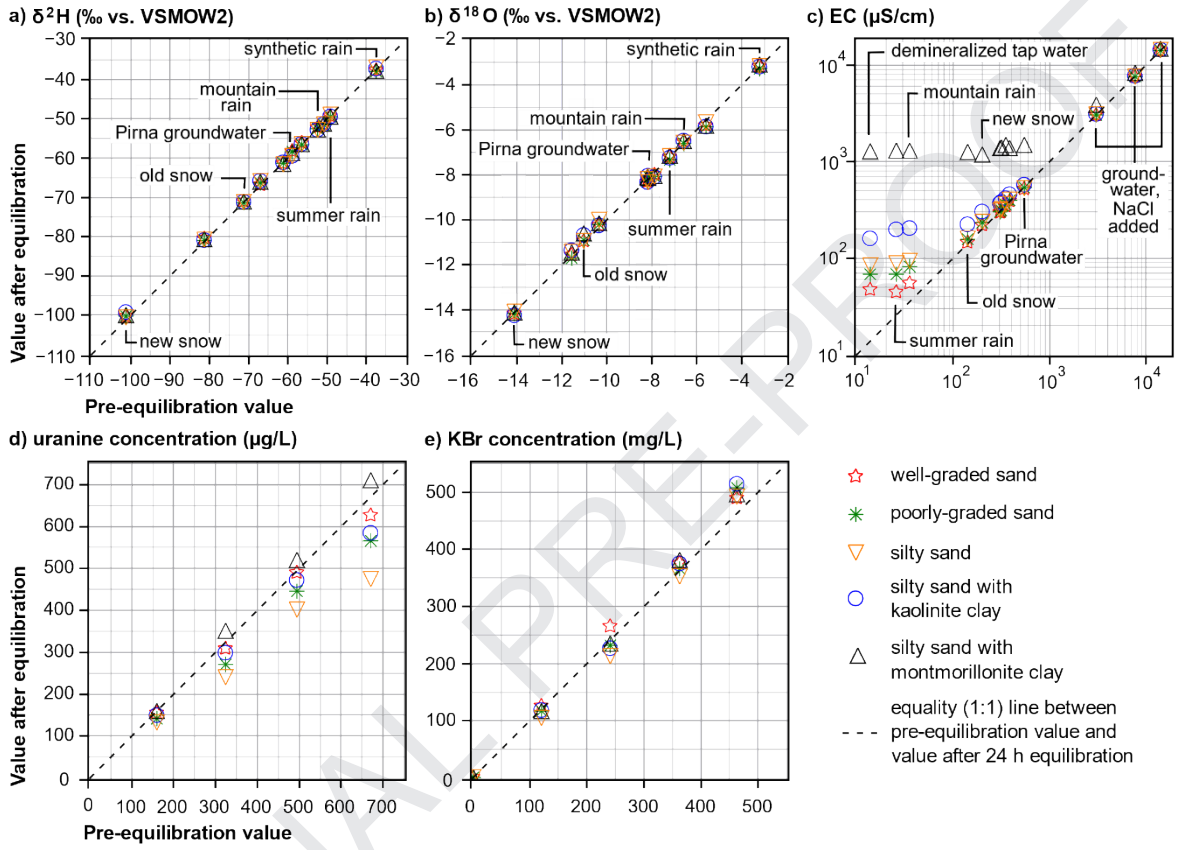



**Figure 2**. Scatter plot of the 24 h stability batch experiments for **(a)** $\delta^{2}H$, **(b)** $\delta^{18}O$, **(c)** EC, **(d)** uranine-induced fluorescence (not corrected to the pH value) as well as **(e)** KBr concentration (ISE method). To improve visibility, the precision of the isotope analysis is not shown. Data points without further description represent mixtures between Pirna groundwater and the precipitation water samples.

As precipitation waters typically have a rather low ionic strength compared to the groundwater, monitoring the EC potentially provides complementary information, especially as it can be effectively monitored at low cost and nowadays even in-situ and adaptively (Vienken et al., 2017). However, the EC batch results with the low-mineralized waters frequently deviated from the 1:1 line, especially in the EC range below ~300 µS/cm, indicating a systematic modification (Figure 2c). Furthermore, these batch samples showed a steady turbidity increase in the water phase. This can presumably be attributed to changes in the sediment's coagulation capabilities, which, in turn, may be an indicator for a

detrimental impact on the porous media itself. Note that the lowest and highest effect in this regard was observed for the well-graded sand and the sample with montmorillonite, respectively, and that the $Y_{Batch}(\log EC_{low})$ value of ~0.58 that was determined for these waters was the maximum value in this study. These observations can be explained by water-sediment reactions: By replacing the natural pore water with precipitation water, i.e., with a typically under-saturated solution, mineral dissolution and, to a minor extent, also ion exchange may increase the pore water's EC during re-equilibration (e.g., Appelo and Postma, 2010). Representing the natural conditions, no significant change was observed for the EC batch experiments with unaltered Pirna groundwater. The symbols are almost on the 1:1 line except for the non-native sample with montmorillonite where EC increased drastically to ~1 mS/cm. Waters with higher initial ionic strengths were found to remain stable, i.e., the difference between initially applied and measured EC remained negligible compared to its absolute value. For example, the $Y_{Batch}(\log EC_{NaCl})$ value was only ~0.10 for these experiments with NaCl added to the groundwater.

In comparison, uranine results were affected by sorption ($Y_{Batch}$(uranine) value of ~0.21, Figure 2d), as previously observed (Fichtner et al., 2015). Furthermore, the fluorescence signal itself showed a non-ideal behavior. Specifically, a signal increase beyond the initial value was observed for the samples containing montmorillonite (black upwards triangles in Figure 2d), highlighting a strong relationship between the measured fluorescence and the solutions' pH value. Here, an increase from pH 7 to near pH 10 was observed for all samples, which can be explained by the $NaHCO_3$ pre-treatment of the 'Friedländer Blauton'. Finally, KBr showed a relatively high stability even though the concentration-dependent accuracy of the ISE method employed is clearly visible (Figure 2e). This is expressed by the still small $Y_{Batch}$(KBr) value of ~0.08. This result lies in-between the results observed for the isotopes, NaCl and uranine and far below the inverse EC-based stability values. Reference measurements employing the IC method for selected samples point towards lower $Y_{Batch}$ values (data not shown).

*4.2. Column transport experiments E1 to E3*

Results for the experiments E1 to E3 are shown as concentration-normalized BTCs in Figure 3, together with the corresponding results of the inverse model simulations (ESM S2).

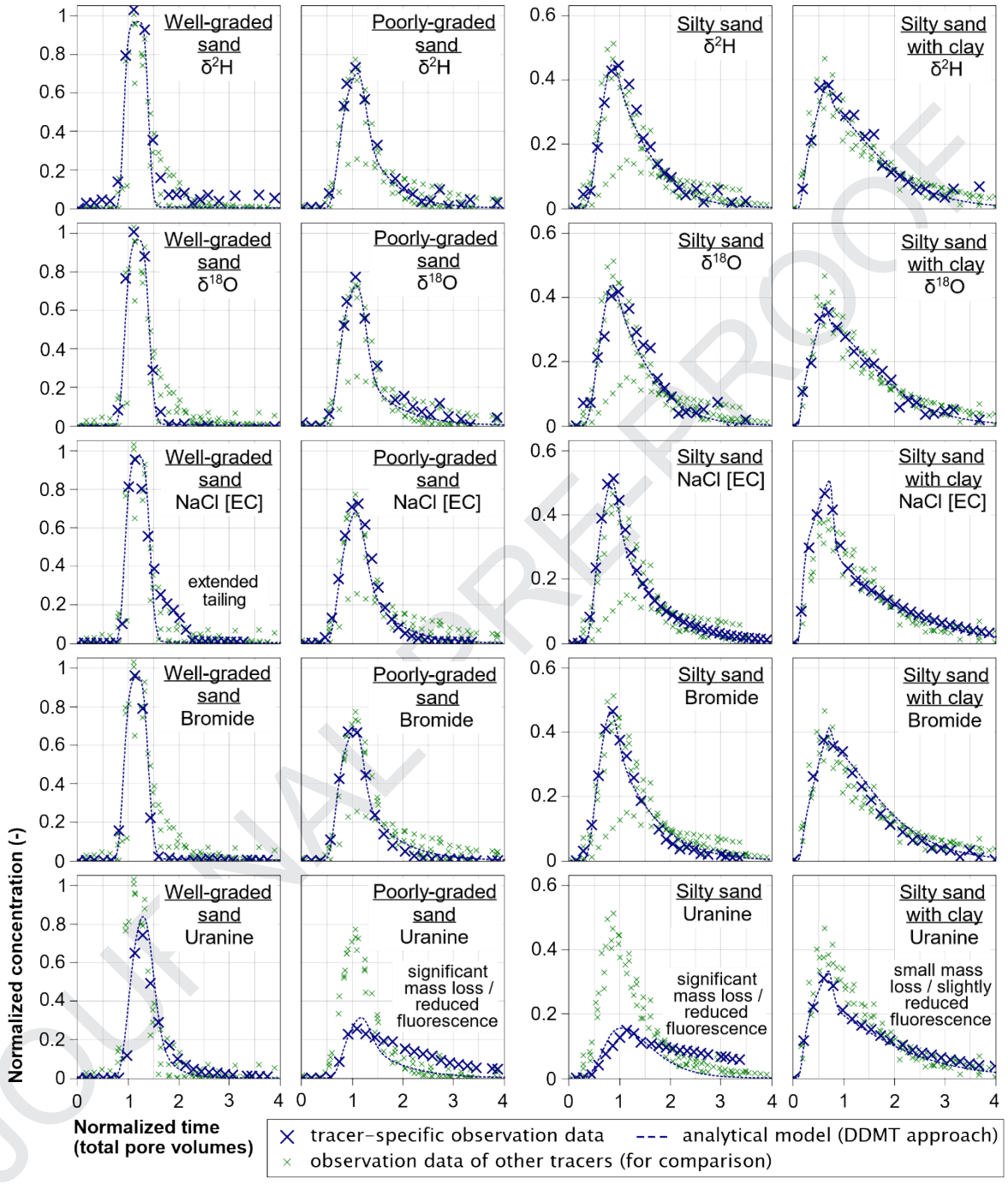



**Figure 3**. Normalized tracer BTCs, based on analytical mean values, as well as corresponding best-fit model simulations. Normalization was done using the simplified Eq. 2, whereby values below 0% are not displayed. Time series are corrected with respect to dead volumes and given in a normalized form. Please also note that the concentration scales differ.

Almost all applied tracers achieved a full breakthrough within the primary experimental period of ~8 days, which corresponds to ~4 exchanged total pore volumes. The only exemption was uranine in the silty sand column, which showed excessive tailing. As

expected, the BTCs for well-graded sand (Figure 3, 1st column) have the narrowest shape and highest peak values where the normalized concentration peak value reached almost 100% of the amended tracer amplitude. Furthermore, the BTC shape widens for the poorly-graded sand (2nd column) and even further for both the silty sands without (3rd column) and with kaolinite clay (4th column), owing to the increasing hydrodynamic dispersion caused by the increased pore-scale variability of *K* values and, thus, also flow velocities. Correspondingly, observed peak concentrations as well as first arrival times decrease with increasing non-uniformity of the sediments.

In terms of the tracer-specific migration behavior the results of the column experiments largely reflect the results from the batch experiments. As expected, the breakthrough of the isotopically enriched synthetic rain (E2) was associated with increased $\delta^2H$ and $\delta^{18}O$ values (Figure 3: 1st and 2nd row). However, isolated values slightly exceeded the expected range spanned by the background's and tracer's signature. In the silty sand experiment, the isotope peak was slightly retarded, and the peak value was reduced compared to both NaCl and KBr, while the times of first arrival did not differ. A possible explanation might be a higher matrix diffusion rate as the water molecules are smaller in size. Although there were no negative observations for KBr (4th row), it should be noted that the more accurate IC method was employed here, while the ISE method was used for the batch tests. Extended tailing was observed for the NaCl application in the well-graded sand (3rd row, separately marked). Furthermore, the normalized EC peak for the silty sand experiment with clay was significantly higher compared to the other studied tracers. This can be explained by cation exchange reactions on the sediments, combined with ion-specific sorption, as previously reported (Mastrocicco et al., 2011; Singha et al., 2011). Nevertheless, despite this slightly non-ideal behavior of NaCl and method-specific uncertainties of KBr, both salt-based tracers can still be considered as effectively stable tracer substances. In contrast, the uranine breakthrough was strongly affected by non-ideal physicochemical behavior, including a retarded arrival, a smaller peak value and stronger tailing (Figure 3, 5th row). This suggests that uranine transport was most likely affected by sorption, even in the experiments with the

well-graded sand. This behavior was even more exaggerated for the poorly-graded sand and the silty sand. In addition, the calculated mass recoveries were limited to ~65% and ~70%, respectively. The breakthrough in the kaolinite sample was less affected. This phenomenon may be mainly attributed to different sediment compositions (Table 1 and Figure 2d). Overall, uranine performed in an unpredictable manner and must be classified as a non-suitable tracer, at least in the context of the conditions for the groundwater and mineralogy being present in Pirna.

In general, the relatively small differences in concentration peak value and tailing behavior among the investigated tracers resulted in correspondingly small ranges for the transport parameters obtained by the inverse modeling procedure for the respective sediments. In particular, the immobile porosity, dispersivity and mass transfer values obtained for the $\delta^{2}H$ and $\delta^{18}O$ data were mostly close to the mean value obtained for all tracers, with a slight tendency towards the respective observed minimum values (ESM S2). All quality criteria showed a good fit among the tracers, with exception of uranine. Based on the normalized BTCs, the average RMSE was 5.6% (min: 2.4%, max: 11.3%) and MAE was 4.2% (min: 1.9%, max: 8.6%), while $wR^2$ spanned a range from 0.73 to 0.98 ($\bar{x}$: 0.86) and the index of agreement from 0.95 to 1.00 ($\bar{x}$: 0.98). Uranine datasets were again excluded, as they differed significantly. Linear regression line slopes were found to be between 0.79 and 1.20 with a mean value of 0.97 being near to the optimal value of '1', again except for uranine. More details including the omitted uranine values are provided in ESM S3.

*4.3. Column transport experiments E4 to E6*

The overall results of the natural precipitation water experiments E4 to E6 (Figure 4) were generally similar to the results obtained for the synthetic rain sample using stable isotope analysis (E2) and for the NaCl application using EC for breakthrough detection (E1). However, as the absolute isotopic shift of the injection water was much less pronounced compared to the E2 experiment, a much coarser resolution of the BTCs was observed. Similar to E1, the breakthroughs of the precipitation waters were associated with significant

EC changes; however, this time in the opposite direction (Figure 4c). While EC peaks were observed at almost the same time as the isotopes, an information loss was evident as the normalized peak value of these inverse EC BTCs reached only ~80% to ~90% of the corresponding isotope peak (see theoretical peak values in Figure 4c). Both observed transport phenomena are therefore further discussed.

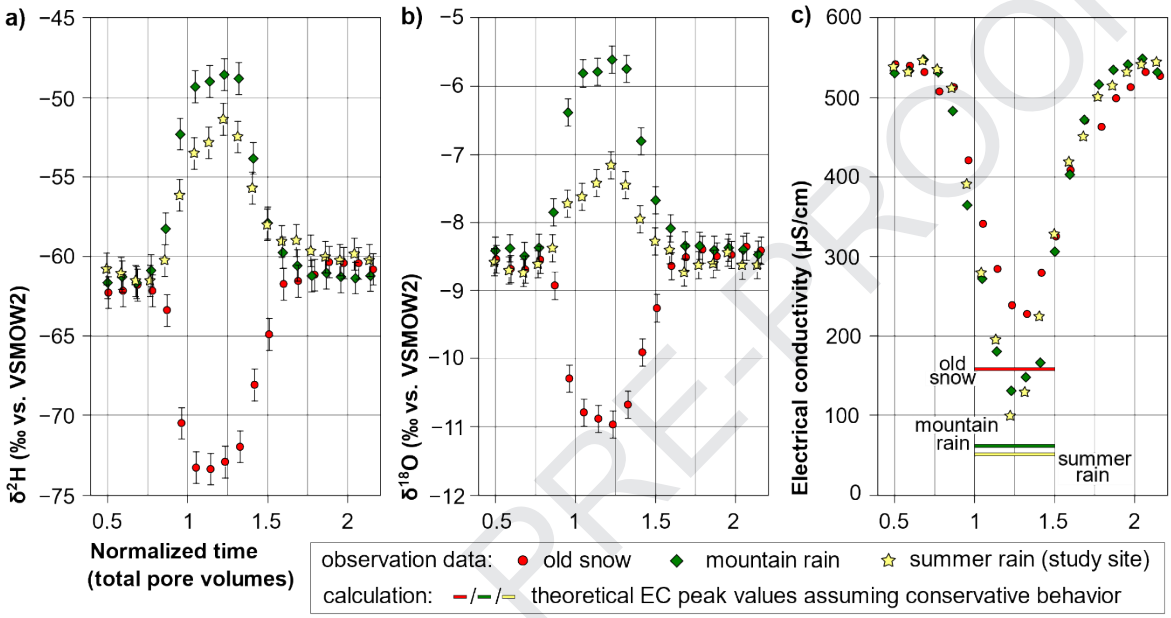



**Figure 4:** Temporal behavior of **(a)** $\delta^2H$, **(b)** $\delta^{18}O$ and **(c)** EC measured at the outflow of the sand column after separate injection of either old snow, mountain rain or summer rain. IRMS precision is shown as vertical error bars in graphs **(a)** and **(b)**. The horizontal lines in graph **(c)** mark the theoretical peak values for EC assuming the same migration behavior as the isotopes.

## 5 Detailed analysis of the observed transport phenomena

### *5.1. Influence of stable isotope analysis precision*

For the synthetic rain sample (experiment E2), the tracer's SNR values for $\delta^2H$ and $\delta^{18}O$ were ~26 and ~28.5, respectively, which resulted in high resolution BTCs (Figure 3, except for some minor outliers). This SNR calculation was based on an initial tracer shift of $\Delta(\delta^2H) \approx 26‰$ and $\Delta(\delta^{18}O) \approx 5.7‰$ versus the reported IRMS precision of ±1‰ ($\delta^2H$) and ±0.2‰ ($\delta^{18}O$), respectively. The tracer SNRs within the series with natural precipitation waters, however, decreased to significantly smaller values, in some cases to values close to and even below 10. Given these conceptional differences, IRMS precision was included in the BTC normalization procedure using Eq. 3 instead of Eq. 2. The resulting normalized BTCs and the corresponding precision confidence intervals are shown in Figure 5.

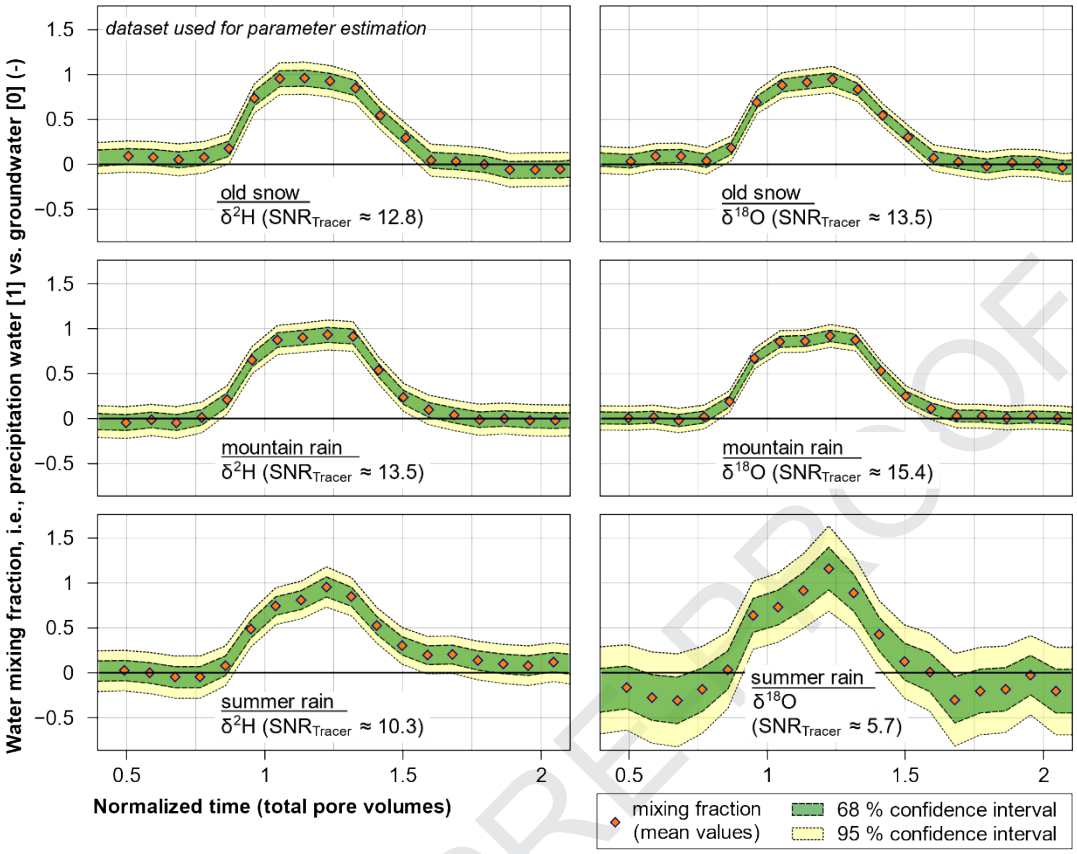



**Figure 5**. Normalized BTCs for the old snow sample and the two rain samples, considering a normalization uncertainty due to IRMS precision for signatures of samples, tracer as well as background. For simplification, constant precision errors were assumed.

The BTC shapes of the old snow, of the mountain rain and, accepting a slightly higher uncertainty, also of the $\delta^2H$ component of the summer rain are still smooth and characterized by a rather small error margin. In contrast, the normalized BTC for the summer rain $\delta^{18}O$-experiment, characterized by the low initial SNR, became highly unstable and noticeably exceeded the possible mixing fraction range (0 to 1). It is evident that even slight deviations from the 'true' value can lead to an inaccurate and unsteady normalization. Eventually, this is attributed to the technically limited accuracy. Such small deviations can be caused, among other reasons, by random and unavoidable errors during sampling itself and by simple rounding errors due to the device-limited measurement resolution.

In order to illustrate the effects of low SNRs on the quality of parameter estimation, a transport parameter calibration was performed for the old snow experiment and multiple SNR scenarios (Table 7), each constrained by the observed $\delta^2H$ breakthrough data (marked in Figure 5). For this purpose, the standard advection-dispersion equation (ADE) was

applied in combination with a simple Monte-Carlo approach. A large range of BTCs (~5300 simulations), each based on mobile porosity and longitudinal dispersivity values randomly selected from a predefined range, was generated and eventually superimposed to define the BTC envelopes. The parameter range definition was manually adjusted until these envelopes approximately matched most of the measured data points during the peak, including their error margins.

**Table 7.** Impact of low SNRs on parameter estimation using a simple ADE (example: well-graded sand, application of the old snow sample, $\delta^2H$ BTC dataset).

| assumed precision (‰) | SNR during peak (‰/‰) | range for mobile porosity (%) | range for longitudinal dispersivity (cm) | comment |
|---|---|---|---|---|
| ±0.0 | ∞ | 31.7–31.8 | 0.17–0.18 | no errors (diamonds in Figure 5) |
| ±0.5 | 25.2 | 31.7–31.8 | 0.13–0.25 | - |
| ±1.0 | 12.6 | 31.3–32.0 | 0.11–0.45 | standard laboratory error (~ green areas in Figure 5) |
| ±1.5 | 8.4 | 31.1–32.2 | 0.08–0.66 | - |
| ±2.0 | 6.3 | 30.7–32.5 | 0.07–0.95 | doubled laboratory error (~ light yellow areas in Figure 5) |
| ±3.0 | 4.2 | 30.4–33.0 | 0.07–1.4 | - |
| ±4.0 | 3.2 | 30.0–33.5 | 0.06–2.3 | - |
| ±5.0 | 2.5 | 29.3–34.1 | 0.05–3.4 | - |

The experiments demonstrate the importance of providing a clear isotopic contrast between injection and background water in order to obtain a sufficiently resolved breakthrough signal at the sample location. Any increase or decrease of measurement uncertainty (here: the IRMS precision) clearly affects the shape of each analyzed BTC. Errors are then further propagated, which influences the parameter calibration process, eventually leading to an increased or decreased bandwidth for all transport parameters, respectively. The actual impact, however, also depends on the examined parameter. Specifically, the results of the parameter estimation procedure (Table 7) show that the

influence of the precision is much smaller for the mobile porosity than for the longitudinal dispersivity, especially for values representing higher laboratory errors.

Considering the results, a minimum SNR during the peak breakthrough of at least 10, preferably higher, is suggested to effectively limit uncertainty during parameter estimation. For advection-dominated 1-D systems (sand column) and assuming sufficient amounts of injected tracer mass, peak values may only be slightly decreased as compared to the initial isotopic shift relative to the background. Hence, the previously mentioned ratio may be directly applied to the initial shift. However, higher initial SNRs (during tracer application) are required for columns with increased dispersive and non-equilibrium transport components (e.g., both silty sand columns) in order to obtain BTCs with reasonable resolutions.

Note that this laboratory-derived recommendation for minimum SNRs may not be directly applicable for field-scale applications as the tracer mass (here: the amount of precipitation water) required to achieve a reasonable resolution may increase beyond technical feasibility, at least for realistic isotopic shifts of natural waters. The only exception to this finding may apply to short-term and short-distance applications such as a push-pull test. For the Pirna study site one such example is documented in ESM S4, in comparison to an injection test with following drift phase and to a two-well test. While mainly depending on the envisaged BTC resolution during the peak and on the technically feasible initial isotopic shift, modeling results of ESM S4 indicate, in turn, that the amount of required injection water also depends on the injection method itself.

*5.2. Reaction-induced modifications of electrical conductivity*

By employing the hydrogeochemical simulation software PhreeqC (Parkhurst and Appelo, 2013), a series of 1-D numerical experiments was performed to reproduce the EC information loss, i.e., the reduction of the normalized peak value as observed in the transport experiments E4 to E6 (Figure 4c). For these simulations, a virtual 1-D column was set-up, discretized into 200 equidistant mobile cells, and each linked to a stagnant cell representing the immobile zone. The initial pore water chemistry was defined according to the chemical

composition of the Pirna groundwater (ESM S1). Initial ion exchanger compositions and mineral saturation states were calculated assuming equilibrium with the pore water. The actual transport simulations were then performed as 1-day injection pulses of water with low ionic strength comparable to the employed rain in the laboratory experiments (composition adapted from Appelo and Postma, 2010). The injection of virtual rain was followed by a continuous flushing period with Pirna groundwater. Note that this numerical investigation focused solely on the variation of selected reaction types as already implemented in the standard reaction database of PhreeqC. Specifically, carbonate mineral reactions, ion exchange, and dual-domain mass transfer were analyzed regarding their potential impact on the model result. Reaction parameters including pH value were varied as listed in Table 8. Physical transport parameters (e.g., porosities) were taken from the parameter estimation results for the well-graded sand experiment (ESM S2) and kept constant for all model runs. Further reaction-induced variations of the porous media properties were not considered, as this would require thermal–hydraulic–mechanical–chemical, i.e., THMC capabilities of the reaction code.

**Table 8**. Parameter ranges for ion exchange, mineral reactions, pH value offsets and non-equilibrium mass transfer rates employed for the 1-D reactive transport simulations.

| reaction parameter | investigated parameter range | |
|---|---|---|
| | main analysis | selected scenarios |
| capacity of ion exchanger (mmol/L) | 0–60 | up to 120 |
| carbonate mineral phase concentration (mmol/L) | 0–2 | up to 200 |
| pH value offsets (-) [a] | 0–0.9 | 1.2 and 1.4 |
| dual-domain, non-equilibrium mass transfer (1/d) | 0.001 and 0.1 | 0.01 |
| ionic strength of applied rainwater (mmol/$kg_W$) | ~0.3 | ~0.6 |

[a] relative to initially defined groundwater-saturated conditions, i.e., $pH_{gw}$ - $pH_{prec}$

In general, the model output indicates that mineral reactions, in combination with a sufficiently pronounced pH value offset relative to the ambient pore water, are most likely the main contributors to the observed EC modifications. Even for pH value offsets below 1 and comparably low mineral phase concentrations up to ~1 mmol/L, i.e., a still realistic range for the investigated sand column setup and the applied rainwater-groundwater combination,

the EC modification is already significant (Table 9). Calculated information losses, i.e., the relative reductions in the peak value cover a range between ~5% and ~19%, which fits the experimentally observed values. This behavior is further intensified with increasing pH value offset (data not shown). For example, the reductions were 30% and 40% in the scenarios with mineral phase concentrations of ~2 mmol/L and pH value offsets of 1.2 and 1.4, respectively. There is a transition range between ~0.06 and ~0.2 mmol/L, where the simulation of the mineral reaction proceeds stepwise, eventually leading to two superimposing, sometimes still distinguishable BTC peaks (Table 9). Note that for the investigated pH range, peak reductions remained stable also for scenarios with higher mineral phase concentrations up to 200 mmol/L. Contrary, the information loss is negligible (≤ 2%) for all scenarios with mineral concentrations lower than 0.04 mmol/L.

**Table 9**. Calculated information losses relative to a conservative tracer. Given are selected results for a dual-domain mass transfer rate of 0.1 $d^{-1}$ and an ionic strength of 0.3 $mmol/kg_w$ for the rainwater.

| **mineral phases (mmol/L)** | **exchanger capacity (mmol/L)** | **relative peak reduction in %** with $pH_{gw}$ - $pH_{prec}$ | | | | | |
|---|---|---|---|---|---|---|---|
| | | 0 | 0.2 | 0.4 | 0.6 | 0.8 | 0.9 |
| 0 | all scenarios | ~1% and less | | | | | |
| 0.02 | all scenarios | between 1.3% and 1.5% | | | | | |
| 0.04 | all scenarios | between 1.6% and 1.7% | | | | | |
| 0.063 | 0 | 4.8 | 2.6/~6[a] | 2.0/~8[a] | 1.9/-[a] | 1.9/-[a] | 1.9/-[a] |
| | 30 | 5.2 | 2.2/~6[a] | 2.0/~8[a] | 1.9/-[a] | 2.5/-[a] | 1.9/-[a] |
| | 60 | 5.2 | 2.2/~6[a] | 2.0/~8[a] | 1.9/-[a] | 1.8/-[a] | 1.9/-[a] |
| 0.1 | 0 | 4.8 | 5.9 | 7.8 | 2.9/~11[a] | 2.5/-[a] | 2.4/-[a] |
| | 30 | 5.2 | 6.3 | 8.0 | 2.8/~11[a] | 2.5/-[a] | 2.4/-[a] |
| | 60 | 5.2 | 6.4 | 7.9 | 2.8/~11[a] | 2.5/-[a] | 2.4/-[a] |
| 0.2 | 0 | 4.8 | 6.0 | 7.8 | 10.8 | 15.1 | 8.2/~17[a] |
| | 30 | 5.2 | 6.4 | 8.3 | 11.3 | 15.1 | 6.1/~17[a] |
| | 60 | 5.2 | 6.4 | 8.4 | 11.4 | 15.2 | 6.1/~17[a] |
| >1 | 0 | 4.8 | 6.0 | 7.9 | 10.8 | 15.1 | 18.0 |
| | 30 | 5.2 | 6.4 | 8.3 | 11.3 | 16.0 | 19.1 |
| | 60 | 5.2 | 6.4 | 8.4 | 11.4 | 16.0 | 19.2 |

[a] two superimposing peaks → range between 'outer peak' (1st value) and, if distinguishable, the 'inner' peak (2nd value)

The normalized EC signal is further modified when ion exchange is additionally simulated, with relative changes up to 5% (observed at a pH offset of 1.4). However,

exchanger capacities of more than 60 mmol/L have no additional effect on the simulation results and systems without mineral reactions seem to be not affected at all by ion exchange. At least for the simulated sand column (small immobile fraction), the influence of dual domain mass transfer on the EC information loss is negligible, with deviations of less than ±1% (not shown in Table 9). Almost the same applies for the ionic strength of the injected rainwater pulse. On a relative scale, higher ionic strengths of the pulsed injection water may eventually lead to a slightly more dampened normalized EC signal. However, the effective differences in the information loss are below 2% when comparing the two investigated ionic strengths.

In summary, the discussed processes form a rather complex reaction system showing a non-linear correlation between the parameters and their contribution to the accompanying EC modification. Nevertheless, additional EC measurements can eventually assist to slightly increase the accuracy that is achievable by parameter estimation, at least indirectly, as the EC observations due to precipitation water migration can serve as simultaneous constraints.

## 6. Conclusions

This study showed that precipitation waters are generally suitable as injection waters in artificial tracer tests for characterizing the flow and transport conditions in groundwater systems over short distances and where experiments are limited to a relatively short duration. Here, they can be employed as valid substitutes to pure deuterium oxide or water-$^{18}O$ avoiding an extensive everyday use of these often highly concentrated isotope tracers in order to preserve the natural signatures that persist in the environment.

The experimental results confirm the strongly conservative behavior of the two water isotope tracer components, while, in contrast, the benefit of measuring and interpreting EC signals is far less clear, even as an auxiliary tracer. This results mostly from the occurrence of water-sediment reactions that would typically be triggered by the mineral under-saturation of the precipitation water.

The isotope-related simulations illustrate the need for considering the uncertainties induced by the technical limitations of stable isotope analysis, as they clearly affect the

inversion process that extracts the hydrogeological properties from the collected multi-tracer data. A universally valid recommendation for the required initial isotopic difference between tracer and background cannot be provided. However, a suggestion for this required difference can be derived from pre-experimental conservative model simulations. Hereby, approximately a SNR of 10 as target value during the breakthrough peak might be considered as a possible 'rule of thumb'. The supporting EC-related model simulations clearly confirmed the need for using appropriate reactive transport codes to include the peak modifications if EC is employed as an additional constraint.

Future research should focus on the influence of analytical precision for parameter estimation in the context of field-scale tracer applications in heterogeneous aquifers. Due to the relatively high analytical costs that are associated at least with the still prevalent IRMS systems, a data worth analysis (e.g., Wallis et al., 2014) should be performed to define optimized sample amounts and frequencies. Finally, more detailed investigations should be envisaged to clarify possible EC signal changes during the use of precipitation waters for systems with more significant non-equilibrium conditions.

**Supplementary materials**

Additional information is provided in the ESMs S1 ("Experimental schemes and groundwater sampling details"), S2 ("Comparative parameter estimation for the laboratory column tests with synthetic rain"), S3 ("Statistical analysis for the laboratory column tests with synthetic rain") and S4 ("Field-scale simulations for precipitation water applications"). The experimental data shown in the Figures 2, 3 and 4 is digitally provided via Figshare (Binder et al., 2019b).

**Acknowledgments / funding information**

Joanne Vanderzalm and Luisa Schmidt are thanked for providing critical internal reviews. Furthermore, Patricia Stock, Thomas Fichtner, Fritz-Florian Kalwa, Stephan Seibert, James Jamieson, Adam Siade, Charles Werth, Robert Pinzinger and Stephan Klotzsch are

acknowledged for their participation in scientific discussions. We would also like to thank the staff members of the Institute of Groundwater Management for their support.

This study was funded by the German Research Foundation (grant numbers BU 3083/3-1, LI 727/24-1, DI 833/17-1, WA 3973/6-1, INST 269/436-1 FUGG). Travel funding for two research stays (Commonwealth Scientific and Industrial Research Organisation; University of Western Australia) was awarded by the TU Dresden Graduate Academy and by the German Academic Exchange Service (great!ipid4all project ID 2016_55).

**References**

Adomako, D., Maloszewski, P., Stumpp, C., Osae, S., Akiti, T.T., 2010. Estimating groundwater recharge from water isotope ($\delta^2H$, $\delta^{18}O$) depth profiles in the Densu River basin, Ghana. *Hydrolog. Sci. J. 55(8)*: 1405-1416, doi: 10.1080/02626667.2010.527847

Appelo, C.A.J., Postma, D., 2010. *Geochemistry, groundwater and pollution*, 2nd ed. CRC Press: Boca Raton, FL, USA; 649 pp.

Arye, G., Dror, I., Berkowitz, B., 2011. Fate and transport of carbamazepine in soil aquifer treatment (SAT) infiltration basin soils. *Chemosphere 82(2)*: 244-252, doi: 10.1016/j.chemosphere.2010.09.062

Becker, M.W., Coplen, T.B., 2001. Technical Note: Use of deuterated water as a conservative artificial groundwater tracer. *Hydrogeol. J. 9:* 512-516, doi: 10.1007/s100400100157

Binder, M., Tritschler, F., Burghardt, D., Klotzsch, S., Dietrich, P., Liedl, R., Händel, F., 2019a. Technical Note: Application of snowmelt as an active and inexpensive dual isotope groundwater tracer. *Hydrogeol. J.* 27(1): 423-433, doi: 10.1007/s10040-018-01917-6

[dataset] Binder, M., Burghardt, D., Engelmann, C., Tritschler, F., Simon, E., Prommer, H., Dietrich, P., Liedl, R., Händel, F., 2019b. Comparative experiments with precipitation waters, synthetic rain and three classical tracers: Results from batch tests and column tracer experiments. *Figshare*, doi: 10.6084/m9.figshare.7928147

Brady, N.C., Weil, R.R., 2002. *The Nature and Properties of Soils*, 13th ed. Prentice Hall: Upper Saddle River, NJ, USA; 960 pp.

Burton Jr., G.A. Pitt, R.E., 2001. *Storm water Effects Handbook - A Toolbox for Watershed Managers, Scientists, and Engineers,* 1st ed. CRC Press: Boca Raton, FL, USA; 928 p.

Dansgaard, W., 1964. Stable isotopes in precipitation. Tellus 16(4): 436-468, doi: 10.3402/tellusa.v16i4.8993

Davis, S.N, Thompson, G.M., Bentley, H.W., Stiles, G., 1980. Ground-Water Tracers - A Short Review. *Groundwater 18(1)*: 14-23, doi: 10.1111/j.1745-6584.1980.tb03366.x

Dietze, M., Dietrich, P., 2012. Evaluation of vertical variations in hydraulic conductivity in unconsolidated sediments. *Groundwater 50(3)*: 450-456, doi: 10.1111/j.1745-6584.2011.00854.x

Fichtner, T., Dong, L., Stefan, C., 2015. Influence of environmental conditions on the stability of dye tracers Brilliant Blue FCF, Uranine and Eosine Y. In: 42nd IAH Congress (AQUA2015), Rome, Italy, 13.09-18.09.

Garnier, J.M., Crampon, N., Préaux, C., Porel, G., Vreulx, M., 1985. Traçage par 13C, 2H, I- et uranine dans la nappe de la craie sénonienne en écoulement radial convergent (Béthune, France). *J. Hydrol. 78*: 379-392, doi: 10.1016/0022-1694(85)90114-3

Greskowiak, J., Prommer, H., Massmann, G., Nützmann, G., 2006. Modeling Seasonal Redox Dynamics and the Corresponding Fate of the Pharmaceutical Residue Phenazone During Artificial Recharge of Groundwater. *Environ. Sci. Technol. 40(21)*: 6615-6621, doi: 10.1021/es052506t

Händel, F., Binder, M., Dietze, M., Liedl, R., Dietrich, P., 2016. Experimental recharge by small-diameter wells: the Pirna, Saxony, case study. *Environ. Earth Sci. 75*: 930, doi: 10.1007/s12665-016-5701-7

Hangen, E., Gerke, H.H., Schaaf, W., Hüttl, R.F., 2005. Assessment of preferential flow processes in a forest-reclaimed lignitic mine soil by multicell sampling of drainage water and three tracers. *J. Hydrol. 303*: 16-37, doi: 10.1016/j.jhydrol.2004.07.009

IAEA, 2013. *TECDOC No. 1723: Using Isotopes for Design and Monitoring of Artificial Recharge Systems*. IAEA: Vienna, Austria.

IAEA/GNIP, 2014. *IAEA/GNIP precipitation sampling guide, version 2.02*. The Global Network of Isotopes in Precipitation (GNIP) and IAEA: Vienna, Austria.

James, E.R., Manga, M., Rose, T.P., Hudson, G.B., 2000. The use of temperature and the isotopes of O, H, C, and noble gases to determine the pattern and spatial extent of groundwater flow. *J. Hydrol. 237*: 100-112, doi: 10.1016/S0022-1694(00)00303-6

Käss, W., 2004. *Lehrbuch der Hydrogeologie Vol. 9, Geohydrologische Markierungstechnik*, 2nd ed. Borntraeger: Stuttgart, Germany, 2004; 557 pp.

Koeniger, P., Leibundgut, C., Link, T., Marshall, J.D., 2010. Stable isotopes applied as water tracers in column and field studies. *Org. Geochem. 41(1)*: 31-40, doi: 10.1016/ j.orggeochem.2009.07.006

Limousin, G., Gaudet, J.-P., Charlet, L., Szenknect, S., Barthès, V., Krimissa, M., 2007. Sorption isotherms: A review on physical bases, modeling and measurement. *Appl. Geochem. 22*: 249-275, doi: 10.1016/j.apgeochem.2006.09.010

Luhmann, A.J., Covington, M.D. Alexander, S.C., Chai, S.Y., Schwartz, B. F., Groten, J.T., Alexander Jr., C., 2012. Comparing conservative and nonconservative tracers in karst and using them to estimate flow path geometry. *J. Hydrol. 448-449*: 201-211, doi: 10.1016/j.jhydrol.2012.04.044

Mali, N., Urbanc, J., Leis, A., 2007. Tracing of water movement through the unsaturated zone of a coarse gravel aquifer by means of dye and deuterated water. *Environ. Geol. 51(8)*: 1401-1412, doi: 10.1007/s00254-006-0437-4

Maloszewski, P., Herrmann, A., Zuber, A., 1999. Interpretation of tracer tests performed in fractured rock of the Lange Bramke basin, Germany. *Hydrogeol. J.* 7: 209-218, doi: 10.1007/s100400050193

Mastrocicco, M., Prommer, H., Pasti, L., Palpacelli, S., Colombani, N., 2011. Evaluation of Saline Tracer Performance during Electrical Conductivity Groundwater Monitoring. *J. Cont. Hydrol. 123:* 157-166, doi: 10.1016/j.jconhyd.2011.01.001

Mook, W.G., de Vries, J.J., 2001. *Environmental Isotopes in the Hydrological Cycle – Principles and Applications. Volume I – Introduction.* UNESCO and IAEA: Paris, France and Vienna, Austria; 185 pp.

Parkhurst, D.L., Appelo, C.A.J., 2013. *Description of Input and Examples for PHREEQC Version 3 - A Computer Program for Speciation, Batch-Reaction, One-Dimensional Transport, and Inverse Geochemical Calculations*. U.S. Department of the Interior and U.S. Geological Survey: Washington, D.C., USA and Reston, VA, USA; 519 pp.

Schoen, R., Gaudet, J.P., Bariac, T., 1999. Preferential flow and solute transport in a large lysimeter, under controlled boundary conditions. *J. Hydrol. 215*: 70-81, doi: 10.1016/S0022-1694(98)00262-5

Seibert, S., Prommer, H., Siade, A., Harris, B., Trefry, M., Martin, M., 2014. Heat and mass transport during a groundwater replenishment trial in a highly heterogeneous aquifer. *Water Resour. Res. 50(12)*: 9463-9483, doi: 10.1002/2013WR015219

Singha, K., Li, L., Day-Lewis, F.D., Regberg, A.B., 2011. Quantifying solute transport processes: Are chemically “conservative” tracers electrically conservative? *Geophysics 76(1)*: F53-F63, doi: 10.1190/1.3511356

Tsujimura, M., Abe, Y., Tanaka, T., Shimada, J., Higuchi, S., Yamanaka, T., Davaa, G., Oyunbaatar, D., 2007. Stable isotopic and geochemical characteristics of groundwater in Kherlen River basin, a semi-arid region in eastern Mongolia. *J. Hydrol. 333*: 47-57, doi: 10.1016/j.jhydrol.2006.07.026

Tritschler, F., Binder, M., Händel, F., Burghardt, D., Dietrich, P., Liedl, R., 2019. Methods Note: Collected rainwater as cost-efficient source for aquifer tracer testing. *Groundwater, early view, doi: 10.1111/gwat.12898.*

van Genuchten, M.T., Wierenga, P.J., 1976. Mass Transfer Studies in Sorbing Porous Media I. - Analytical Solutions, *Soil Sci. Soc. Am. J. 40(4):* 473-480, doi: 10.2136/sssaj1976.03615995004000040011x

Vienken, T., Huber, E., Kreck, M., Huggenberger, P., Dietrich, P., 2017. How to chase a tracer – combining conventional salt tracer testing and direct push electrical conductivity profiling for enhanced aquifer characterization. *Adv. Water Resour. 99*: 60-66, doi: 10.1016/j.advwatres.2016.11.010

Wallis, I., Moore, C., Post, V., Wolf, L., Martens, E., Prommer, H., 2014. Using predictive uncertainty analysis to optimise tracer test design and data acquisition. *J. Hydrol. 515*: 191-204, doi: 10.1016/j.jhydrol.2014.04.061

**Author Contributions**

M.B., F.H., D.B., H.P., F.T., R.L., P.D. → conceptualization

M.B., D.B., F.H., E.S. → methodology

M.B., D.B., F.T., C.E. → investigation

M.B., D.B., F.T., F.H. → validation

M.B., F.T., C.E. → formal analysis

D.B. → resources

M.B., F.H., D.B., E.S. → writing (preparation of original draft)

M.B., F.H., D.B., H.P, E.S., C.E., F.T., R.L., P.D → writing (review and editing)

M.B., C.E. → visualization

R.L., D.B., H.P., P.D. → supervision

R.L., D.B., P.D. → project administration

R.L., D.B., P.D. → funding acquisition (general)

R.L., H.P., M.B. → funding acquisition (traveling)

JOURNAL PRE-PROOF

- Precipitation water-inherent information can be used for active tracing purposes.
- Water stable isotopes ($\delta^{2}H$, $\delta^{18}O$) show a high transport stability.
- Isotope precision has a significant impact on calibration parameter certainty.
- Isotope signal-to-noise ratios should not fall below 10 during peak breakthrough.
- EC breakthrough is biased by multiple reactions leading to information loss.

JOURNAL PRE-PROOF